

Polarization-Selective Excitation of Antiferromagnetic Resonance in Perpendicularly Magnetized Synthetic Antiferromagnets

Yoichi Shiota^{1,2,*}, Tomonori Arakawa^{1D},³ Ryusuke Hisatomi,^{1,2} Takahiro Moriyama,^{1,2} and Teruo Ono^{1,2}

¹ Institute for Chemical Research, Kyoto University, Uji, Kyoto 611-0011, Japan

² Center for Spintronics Research Network, Institute for Chemical Research, Kyoto University, Uji, Kyoto 611-0011, Japan

³ National Institute of Advanced Industrial Science and Technology (AIST), National Metrology Institute of Japan (NMIJ), Tsukuba, Ibaraki 305-8563, Japan



(Received 19 April 2022; accepted 27 June 2022; published 14 July 2022)

Unlike ferromagnets, collinear antiferromagnets have two precession modes exhibiting opposite chirality, which enables the use of the polarization degree of freedom of magnons. In this study, we experimentally measure the polarization-selective spectra of magnetic resonance in perpendicularly magnetized synthetic antiferromagnets using a wideband crossed microstrip circuit. The magnetic resonances with right-handed and left-handed precession modes are directly detected, and theoretical analysis and numerical simulations explain the measurement results by considering the difference in the perpendicular magnetic anisotropy and damping constant between the top and bottom ferromagnetic layers. We also show that magnetic excitations with different polarization types can be excited under degeneracy between the two precession modes. Our work suggests that perpendicularly magnetized synthetic antiferromagnet structures provide an attractive platform for manipulating the polarization degree of freedom of magnons.

DOI: 10.1103/PhysRevApplied.18.014032

I. INTRODUCTION

Magnonics is a research field that aims to realize new functional and high-performance devices using collective excitations of ordered magnetic moments, called magnons [1–3]. Because magnons can carry angular momentum, several device concepts for data transport and processing have been proposed and demonstrated, such as spin-wave-based logic gates and neuromorphic and Boolean computing [4–13]. The data in these magnonic applications are encoded by magnon frequency, amplitude, or phase. However, polarization degree of freedom is rarely used to encode data. This is because the magnetic moments in ferromagnets can precess only in a counterclockwise direction with respect to the effective magnetic field based on the Landau-Lifshitz-Gilbert (LLG) equation, and therefore ferromagnetic magnons always possess right-handed chirality. On the other hand, magnon modes with both right-handed and left-handed chirality are allowed in collinear antiferromagnets (AFMs) owing to the antiparallel coupling between two sublattice magnetic moments [14,15], as shown in Fig. 1(a). When these two precession modes are degenerate, arbitrary polarizations, including elliptically or linearly polarized magnons, can be achieved.

Therefore, there has been a growing interest in polarization manipulation using AFM magnons in recent years, and various methods have been theoretically proposed [16–20], including spin-wave field-effect transistors [16, 20] and polarizing and retarding effects through magnetic textures [17]. However, these have yet to be experimentally demonstrated because it is difficult to realize the excitation of coherent AFM magnons owing to their immunity to an external magnetic field. In recent years, coherent spin pumping effects in AFM/heavy-metal heterostructures with Cr₂O₃ or MnF₂ have been observed, and it has been revealed that opposite precession chiralities in AFMs transport the angular momentum with opposite signs [21, 22]. In these experiments, owing to the strong superexchange coupling in crystalline AFMs, a large magnetic field (several teslas or more) is required to break the degeneracy of the two precession modes, and the resonance frequency reaches sub-THz making it difficult to perform the broadband frequency measurements necessary for a deep understanding of AFM dynamics. In synthetic antiferromagnets (SAFs), two antiferromagnetically coupled ferromagnetic layers are separated by a thin nonmagnetic spacer [23–25]. Because the static and dynamic magnetic properties of SAFs can be easily manipulated and detected owing to the relatively weak exchange coupling compared with crystalline AFMs [26], conventional techniques

* shiota-y@scl.kyoto-u.ac.jp

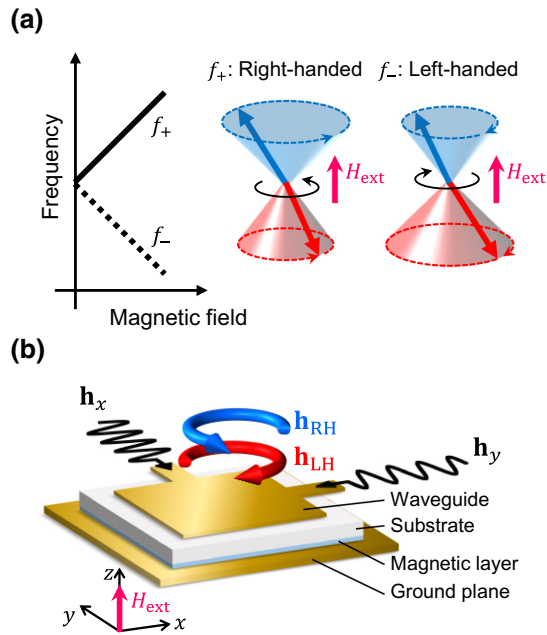


FIG. 1. (a) Illustration of antiferromagnetic resonance modes with right-handed and left-handed circular precession in collinear antiferromagnets. Although the resonance frequencies of the right-handed and left-handed precession modes are degenerate without a magnetic field, they are split into high frequency and low frequency with an applied magnetic field due to the opposite precession chirality. (b) Schematic illustration of our experimental setup with a crossed microstrip resonator. The external magnetic field is applied along the out-of-plane direction.

employed for ferromagnetic materials can be applied [27–35]. Circularly polarized (CP) microwaves are excellent tools for selectively exciting magnetic resonances with different precession chiralities [36]. CP microwaves can be generated from the superposition of two orthogonal linearly polarized microwaves with a difference in phase of $\pi/2$ in time, as schematically shown in Fig. 1(b). To date, experimental demonstrations of selective magnetic excitations and magnetization switching using CP microwaves have been reported [37–42]. However, few studies have directly distinguished the polarization of antiferromagnetic resonance modes, particularly in magnetic thin films.

In this work, the antiferromagnetic resonances in perpendicularly magnetized SAFs composed of two Co/Ni multilayers separated by a Ru thin layer are investigated using broadband and polarization-selective spectroscopy with a crossed microstrip resonator. We first show polarization-selective excitation with a single Co/Ni multilayer to characterize the polarization of the CP microwave field generated by the crossed microstrip resonator. In addition, the magnetic properties of single Co/Ni multilayers with different numbers of repetitions are evaluated. Subsequently, the magnetic resonances with

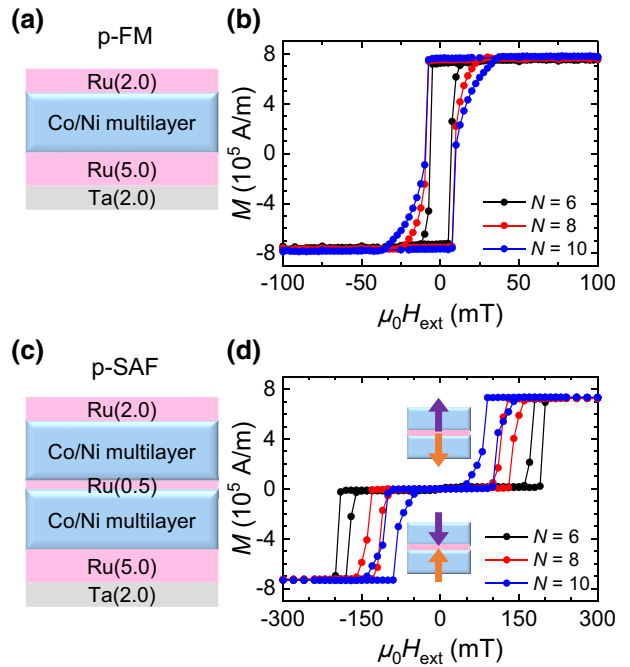


FIG. 2. (a) Film structure of p-FM and (b) M - H loops for different repetition number $N = 6, 8, 10$. (c) Film structure of p-SAF and (d) M - H loops for $N = 6, 8, 10$. The inset of (d) depicts the magnetization configuration of top and bottom Co/Ni multilayers for antiparallel configuration depending on the field sweep direction.

right-handed and left-handed precession modes with perpendicularly magnetized SAFs are directly detected. We find that the crossing field at which the two precession modes degenerate is shifted from the zero field owing to the difference in perpendicular magnetic anisotropy (PMA) between the two Co/Ni multilayers, and this shift field can be modified by changing the stacking repetition number. By comparing the experimental results with numerical simulation, the possible polarizations of the magnetic excitation in our perpendicularly magnetized SAF structure are discussed.

II. EXPERIMENT

Thin films are deposited by dc magnetron sputtering on thermally oxidized Si substrates. We fabricate two types of samples: Ta(2.0)/Ru(5.0)/Co(0.2)/[Ni(0.6)/Co(0.2)] _{N} /Ru(2.0) for perpendicularly magnetized ferromagnets (hereafter referred to as p-FM) and Ta(2.0)/Ru(5.0)/Co(0.2)/[Ni(0.6)/Co(0.2)] _{N} /Ru(0.5)/Co(0.2)/[Ni(0.6)/Co(0.2)] _{N} /Ru(2.0) for perpendicularly magnetized SAFs (hereafter referred to as p-SAF), where the values in parentheses are the thicknesses in nanometers [Figs. 2(a) and 2(c)]. We vary the repetition number N of the Co/Ni multilayer to 6, 8, or 10, which correspond to ferromagnetic layer thicknesses of 5.0, 6.6, and 8.2 nm, respectively. Co/Ni multilayers are chosen because of their high

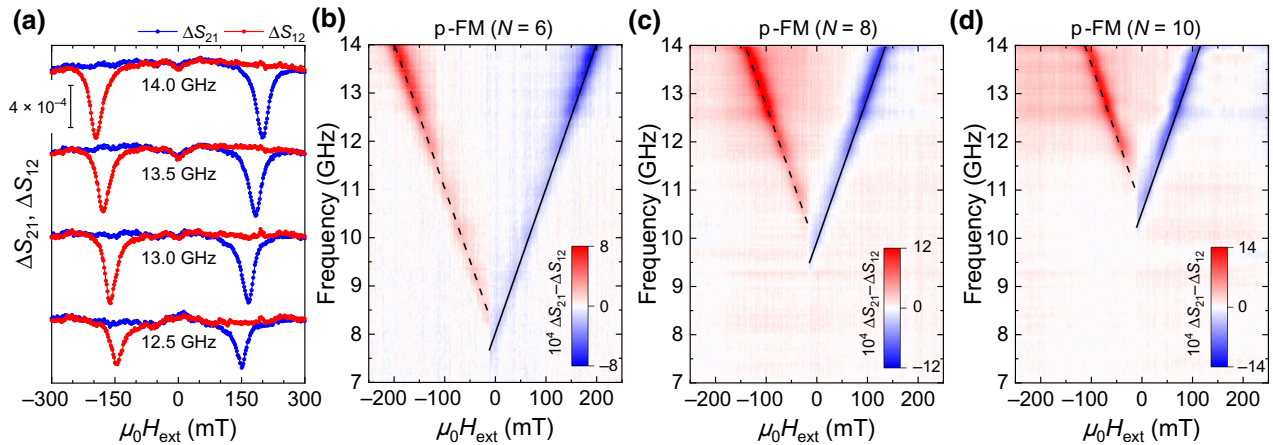


FIG. 3. (a) Spectra of ΔS_{21} (blue) and ΔS_{12} (red) on a perpendicularly magnetized ferromagnet structure with $N = 6$ under various frequencies of 12.5–14.0 GHz. Color plots of $\Delta S_{21} - \Delta S_{12}$ for different repetition number (b) $N = 6$, (c) $N = 8$, and (d) $N = 10$. The external magnetic field is swept from +300 to −300 mT, i.e., a downward field sweep. The solid and dashed lines represent the fit to Kittel's formula.

PMA, large magnetic thickness, and low magnetic damping [43–45]. Figures 2(b) and 2(d) show the out-of-plane magnetic hysteresis loops obtained using a superconducting quantum interference device magnetometer for p-FM and p-SAF with $N = 6, 8$, and 10. For p-FM structures, all samples show full remanent magnetization, indicating a perpendicular easy axis. For the p-SAF structures, both the top and bottom Co/Ni multilayers have perpendicular easy axes, and the magnetic moments between the two layers are fully compensated owing to the interlayer exchange coupling through the Ru(0.5) spacer layer. As the antiferromagnetically coupled exchange field (H_{ex}) is inversely proportional to the thickness of the ferromagnetic layer, the switching field decreases with increasing N . It should be noted that the out-of-plane magnetic hysteresis loops obtained using the magneto-optical Kerr effect (MOKE) in the polar configuration reveal that the tail-to-tail (T-T) or head-to-head (H-H) antiparallel magnetization configurations can be obtained depending on the field sweep direction, as shown in the inset of Fig. 2(d) (see Appendix A for more details).

CP microwaves are generated by the combined method of an overcoupled crossed microstrip resonator and a hybrid coupler developed by Arakawa *et al.* [46]. Broadband and polarization-selective spectroscopy measurements are performed by placing a test sample with an area of $5 \times 5 \text{ mm}^2$ below the square-shaped waveguide, with the magnetic layer side facing the ground plane, as shown in Fig. 1(b). For electrical isolation, the surface of the magnetic layer is covered with sputter-deposited SiO_2 . This setup is positioned between the pole pieces of an electromagnet to apply an out-of-plane magnetic field. Subsequently, two orthogonal microstrip lines are connected to a hybrid coupler (Marki, QH-0226) and vector network analyzer (Keysight, N5224A) through

same-length microwave cables. The hybrid coupler is used as a microwave power splitter, which generates a $\pi/2$ phase shift between the two outputs. The microwave power, intermediate frequency bandwidth, and trace average count of the vector network analyzer are set to 0 dBm (1 mW), 1 kHz, and 10, respectively. The microwave transmission parameters S_{21} and S_{12} are acquired with frequency range 6–20 GHz and step width 0.05 GHz while sweeping the out-of-plane magnetic field. To extract the contribution of the magnetic resonance, we consider the relative change in the magnitude of S_{nm} as $\Delta S_{nm} \equiv |S_{nm}(f, H_{\perp})| - |S_{nm}^{\text{BG}}|$, where $(n, m) = (1, 2)$ are the port numbers and S_{nm}^{BG} is the background signal under the off-resonant field. All measurements are performed at room temperature.

III. RESULTS AND DISCUSSION

We start with p-FM structures to investigate the polarization of the CP microwave field generated by the crossed microstrip resonator and the perpendicular magnetic anisotropy of the Co/Ni multilayers. Figure 3(a) shows the transmission spectra (ΔS_{21} and ΔS_{12}) of a p-FM structure with $N = 6$ measured under various microwave frequencies. The microwave absorption dips for ΔS_{21} spectra are observed in the positive magnetic field region, whereas those for ΔS_{12} spectra are observed in the negative magnetic field region. This indicates that the magnetic resonance is selectively excited, depending on the polarization of the CP microwave field. In our experimental configuration, the microwave output from port 1 of the vector network analyzer generates a right-handed CP microwave field. Conversely, the output from port 2 generates a left-handed field. To visualize the polarization of the magnetic resonance in p-FM structures, color

plots of $\Delta S_{21} - \Delta S_{12}$ are shown in Figs. 3(b)–3(d) for $N = 6, 8$, and 10 in p-FM structures. Because magnetization switching reverses the polarization of the magnetic resonance, the sign of the magnetic resonance peaks is inverted between the positive and negative magnetic field regions. The obtained resonance frequencies as a function of the magnetic field can be explained using Kittel's formula [44], $f = \mu_0\gamma(H_{\text{ext}} + H_k^{\text{eff}})/2\pi$, where μ_0 , γ , and H_k^{eff} are the vacuum permeability, gyromagnetic ratio, and effective PMA field, respectively [see Figs. 3(b)–3(d)]. The estimated $\mu_0 H_k^{\text{eff}}$ values are 268 , 329 , and 353 mT for p-FM structures with $N = 6, 8$, and 10 , respectively.

We next investigate the polarization of the magnetic resonance in the p-SAF structures. Figures 4(a)–4(c) show color plots of $\Delta S_{21} - \Delta S_{12}$ for $N = 6, 8$, and 10 for the p-SAF structures. The upper (lower) results show the spectra obtained from the downward (upward) field sweep, corresponding to the T-T (H-H) antiparallel magnetization configuration. Two precession modes are clearly observed for all samples within the magnetic field range, in which the two magnetizations are antiparallel. It should be noted that the resonance frequencies for the two precession modes show opposite linear dependences on the magnetic field, which is consistent with the dependence expected by considering the sign of the angular momentum of each precession mode. In addition, we find that the crossing field in which the two precession modes degenerate is shifted from the zero field and inverted by changing the antiparallel magnetization configuration.

To analyze these results, we solve coupled LLG equations (see Appendix B for more details) and find the resonance condition of two modes for T-T or H-H antiparallel

TABLE I. Parameters used in calculated resonance frequencies for perpendicularly magnetized synthetic antiferromagnet structures.

N	$\mu_0 H_{k,\text{BL}}^{\text{eff}}$ (mT)	$\mu_0 H_{k,\text{TL}}^{\text{eff}}$ (mT)	$\mu_0 H_E$ (mT)
6	268	368	130
8	329	349	65
10	353	273	20

magnetization configurations as

$$f_{\pm}^{\text{T-T}} = \pm \frac{\mu_0\gamma}{2\pi} (H_{\text{ext}} - \Delta H_k^{\text{eff}}) + \frac{\mu_0\gamma}{2\pi} \sqrt{\bar{H}_k^{\text{eff}}(\bar{H}_k^{\text{eff}} + 2H_E)}, \quad (1)$$

$$f_{\pm}^{\text{H-H}} = \pm \frac{\mu_0\gamma}{2\pi} (H_{\text{ext}} + \Delta H_k^{\text{eff}}) + \frac{\mu_0\gamma}{2\pi} \sqrt{\bar{H}_k^{\text{eff}}(\bar{H}_k^{\text{eff}} + 2H_E)}, \quad (2)$$

where $\Delta H_k^{\text{eff}} = (H_{k,\text{BL}}^{\text{eff}} - H_{k,\text{TL}}^{\text{eff}})/2$ and $\bar{H}_k^{\text{eff}} = (H_{k,\text{BL}}^{\text{eff}} + H_{k,\text{TL}}^{\text{eff}})/2$ are the difference and average of the effective PMA field between the top and bottom ferromagnetic layers, respectively, and H_E is the interlayer exchange field. From Eqs. (1) and (2), the shift in the crossing field is attributed to the difference in PMA between the top and bottom ferromagnetic layers, as reported in previous studies [35,47]. As shown in Figs. 4(a)–4(c), the resonance frequencies expressed by Eqs. (1) and (2) can reproduce our experimental results very well with the parameters shown in Table I. Regarding $H_{k,\text{BL}}^{\text{eff}}$, we used

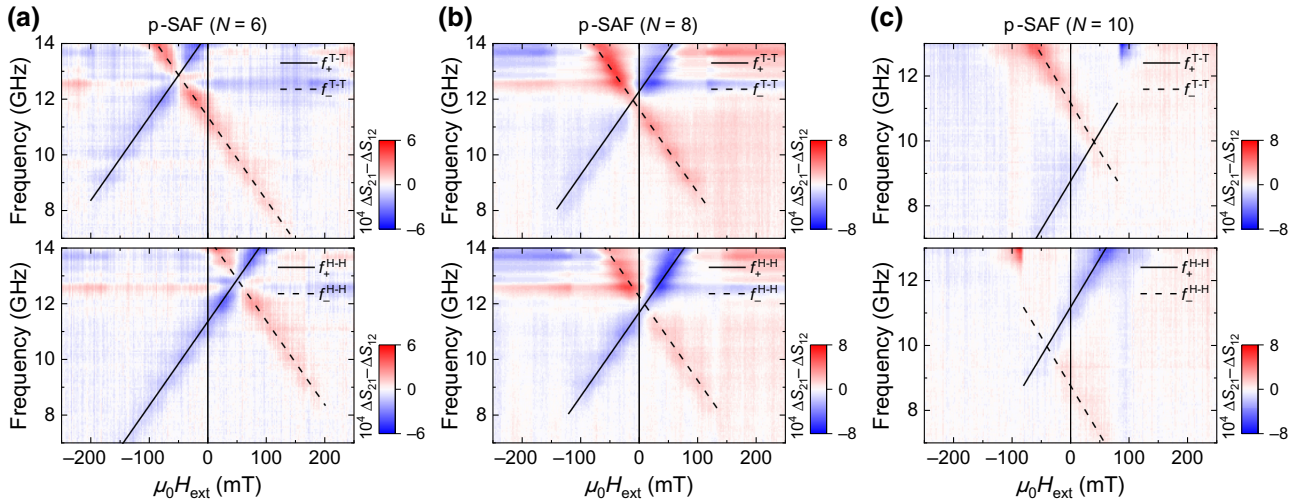


FIG. 4. Color plots of $\Delta S_{21} - \Delta S_{12}$ on perpendicularly magnetized synthetic antiferromagnet structures with (a) $N = 6$, (b) $N = 8$, and (c) $N = 10$. The upper (lower) results show the spectra obtained by downward (upward) field sweep, corresponding to the tail-to-tail (head-to-head) antiparallel magnetization configuration. The solid and dashed lines represent the resonance frequencies calculated from Eqs. (1) and (2) with the parameters in Table I.

the H_k^{eff} values, which are experimentally determined using p-FM structures for each N . As the repetition number N increases, $H_{k,\text{BL}}^{\text{eff}}$ increases while $H_{k,\text{TL}}^{\text{eff}}$ decreases. This may be attributed to the larger surface roughness of the top ferromagnetic layer. The difference in PMA between the two layers is the smallest in the p-SAF structure with $N = 8$.

Figure 5(a) shows the experimentally obtained ΔS_{21} and ΔS_{12} spectra of the p-SAF structure with $N = 8$ at a microwave frequency of 11.95 GHz. We find that the two precession modes are degenerate under $\mu_0 H_{\text{ext}} = 10$ mT, but with different absorption intensities. To gain insights into the observed experimental results, magnetization dynamics with two coupled single-domain magnets are simulated by numerically solving the LLG equation (see Appendix C for more details). The experimentally obtained material parameters for the p-SAF structures with $N = 8$ are used in the simulation. Figure 5(b) shows the calculated precession amplitude spectra under a microwave frequency of 11.95 GHz with right-handed polarization (\mathbf{h}_{RH}) and left-handed polarization (\mathbf{h}_{LH}). We find that different damping constants between top and bottom layer (α_{TL} and α_{BL}) cause a difference in the peak

amplitude, and the calculated spectra reproduce the experimental results when the bottom Co/Ni multilayer has a smaller damping constant [$\alpha_{\text{BL}} = 0.02$ and $\alpha_{\text{TL}} = 0.03$ are used in Fig. 5(b)]. This damping difference may be related to the difference in the growth quality between the top and bottom Co/Ni multilayers due to the surface roughness and/or strain relaxation. The damping constant is often evaluated from the frequency dependence of resonant linewidth. However, this kind of analysis cannot be applied in our measurement due to the frequency characteristic of the crossed microstrip resonator [46]. Therefore, further experimental evidence is needed to discuss the damping constant exactly.

Finally, we discuss the possible polarization of antiferromagnetic resonance under the condition of degeneracy between the two precession modes ($\mu_0 H_{\text{ext}} = 10$ mT, $f = 11.95$ GHz in H-H antiparallel magnetization configuration). Figure 6(a) shows the trajectories of the total magnetization $\mathbf{m} \equiv (\mathbf{m}_{\text{BL}} + \mathbf{m}_{\text{TL}})/2$ under the application of four types of microwave fields (\mathbf{h}_{RH} , \mathbf{h}_{LH} , \mathbf{h}_x , and \mathbf{h}_y), and Figs. 6(b)–6(e) show the detailed evolutions of each magnetization trajectory, including \mathbf{m}_{BL} and \mathbf{m}_{TL} (see Appendix C for the derivation of these variables). Comparing the trajectories when the CP microwave field \mathbf{h}_{RH} or \mathbf{h}_{LH} is applied, the right-handed precession mode has a larger precession amplitude than the left-handed mode. This amplitude difference is due to the different damping constants between the top and bottom ferromagnetic layers ($\alpha_{\text{BL}} = 0.02$ and $\alpha_{\text{TL}} = 0.03$), which is consistent with the results shown in Fig. 5(b). When a linearly polarized microwave field, \mathbf{h}_x or \mathbf{h}_y , is applied, the precession trajectory of \mathbf{m} becomes elliptical with an oscillating component in the direction of the microwave field, which is recombined by the right-handed and left-handed precession modes [48]. These results reveal that p-SAFs provide similar conditions to those of crystalline AFMs and enable the manipulation of magnon polarization [16]. It should be noted that magnetic resonance with perfectly linear polarization can only be realized when the damping constants between the top and bottom ferromagnetic layers are identical (not shown); therefore, it is important to engineer the SAF structure to fully exploit the polarization degree of freedom of the magnon.

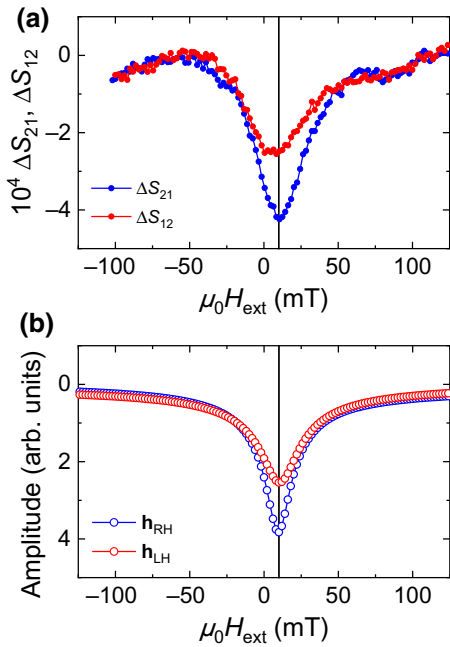


FIG. 5. (a) Experimentally obtained spectra of ΔS_{21} (blue) and ΔS_{12} (red) on a perpendicularly magnetized synthetic antiferromagnet structure with $N = 8$ under fixed frequency of 11.95 GHz obtained by upward field sweep, corresponding to the head-to-head antiparallel magnetization configuration. (b) Calculated precession amplitude of the total magnetization under the application of right-handed circularly polarized microwave field \mathbf{h}_{RH} (blue) and left-handed circularly polarized microwave field \mathbf{h}_{LH} (red). The vertical axis is inverted for comparison with the experimental results.

IV. SUMMARY

We investigate the dynamics of perpendicularly magnetized synthetic antiferromagnets using broadband and polarization-selective spectroscopy with a crossed microstrip resonator. The precession chiralities of the antiferromagnetic resonance are directly distinguished depending on the polarization of the circularly polarized microwave field. We find that the crossing fields in which the right-handed and left-handed precession modes are degenerate are shifted from zero fields, and

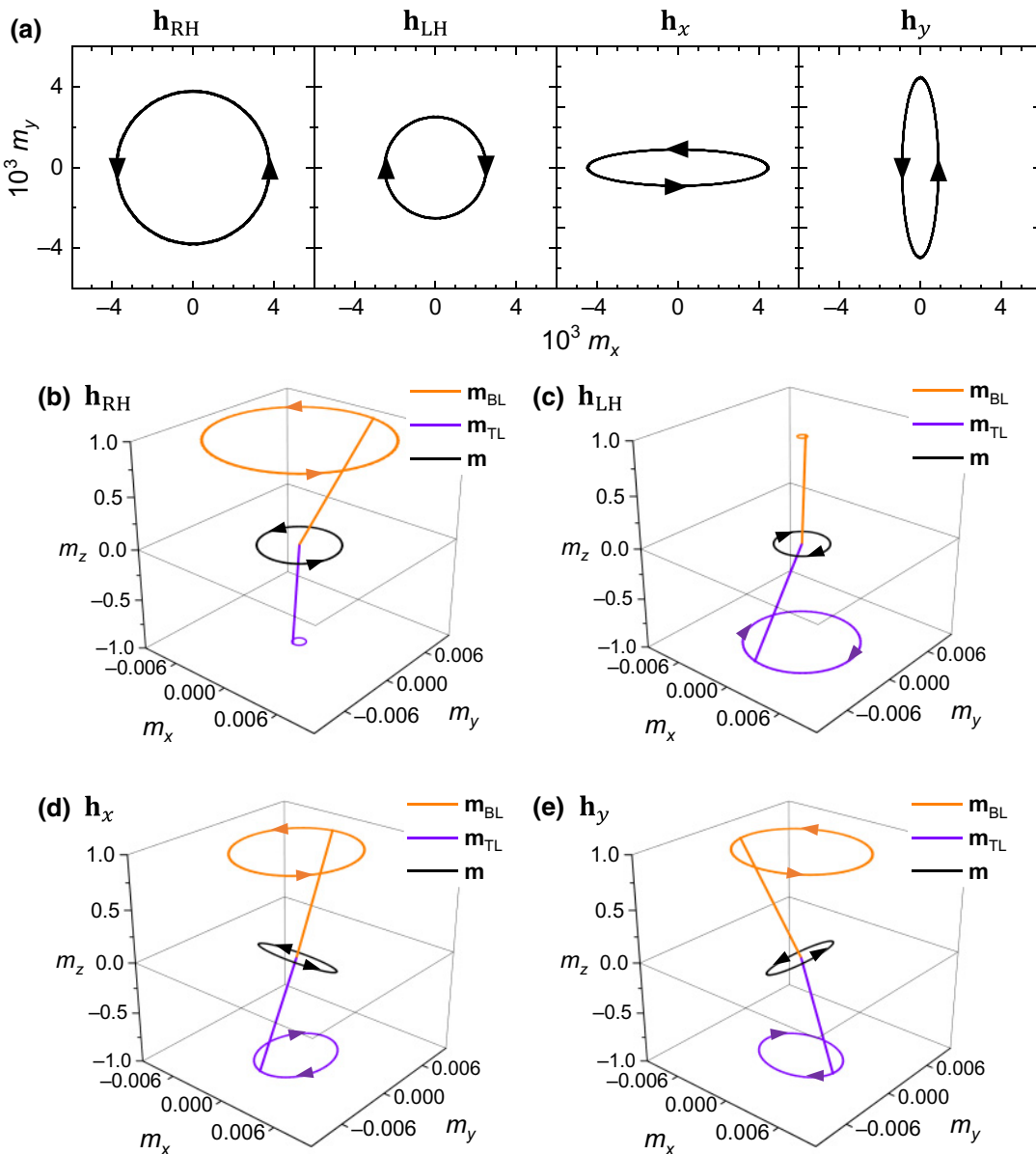


FIG. 6. (a) Calculated trajectories of the total magnetization \mathbf{m} under the application of four types of microwave fields, \mathbf{h}_{RH} , \mathbf{h}_{LH} , \mathbf{h}_x , and \mathbf{h}_y , when the two precession modes are degenerate ($f = 11.95$ GHz and $\mu_0 H_{ext} = 10$ mT in the case of head-to-head antiparallel magnetization configuration). (b)–(e) Corresponding trajectories of \mathbf{m}_{BL} , \mathbf{m}_{TL} , and \mathbf{m} .

the microwave absorption intensities differ between the two precession modes. Theoretical analysis and numerical simulations explain these experimental results by considering the difference in perpendicular magnetic anisotropy and the damping constant between the top and bottom ferromagnetic layers. With the experimentally obtained material parameters, we also discuss the possible polarization of the antiferromagnetic resonance. Our experimental results and analysis could prove valuable for realizing the polarization manipulation of antiferromagnetic magnons based on synthetic antiferromagnets.

ACKNOWLEDGMENTS

This work is partly supported by JSPS KAKENHI Grants No. JP20K15161, No. JP20H05665, No. JP20H00337, No. JP22H01936, No. JP18H01815, and No. JP22H01964 and by the Collaborative Research Program of the Institute for Chemical Research, Kyoto University.

APPENDIX A: MOKE LOOPS FOR p-SAF STRUCTURES

Figure 7 shows the hysteresis loops measured by the MOKE in the polar configuration for p-SAF structures

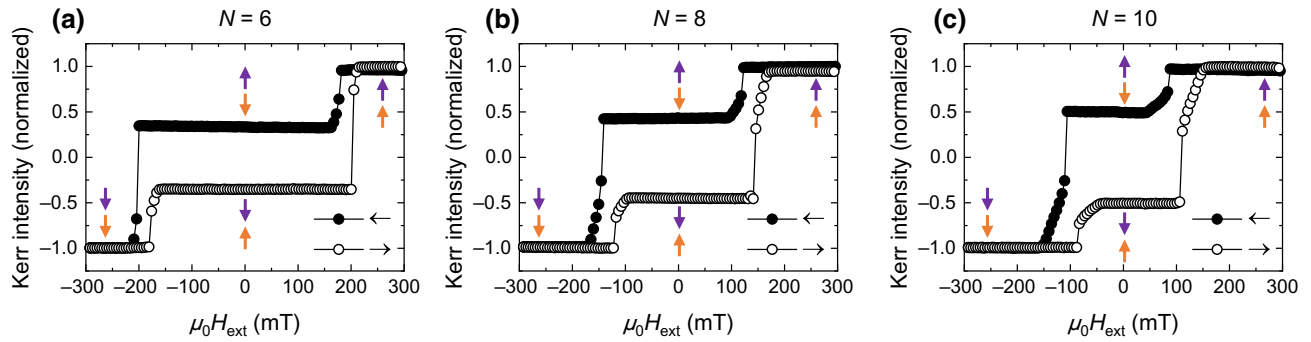


FIG. 7. (a)–(c) MOKE hysteresis loops under a perpendicular magnetic field for perpendicularly magnetized synthetic antiferromagnet structures.

with \$N = 6, 8\$, and \$10\$. Depending on the field sweep direction, there is a Kerr intensity difference within the magnetic field range in which the two magnetizations are antiparallel even though the magnetic moments are fully compensated, as shown in Fig. 2(d). Because the MOKE measurement is a surface-sensitive technique, the change in Kerr intensity associated with magnetization reversal in the bottom layer is smaller than that in the top layer. Based on this consideration and the results shown in Fig. 7, it is clear that when the magnetic field is reduced from the saturated states, magnetization reversal in the bottom layer occurs first in all samples.

APPENDIX B: THEORETICAL MODEL

We consider interlayer exchange-coupled bilayers with perpendicular magnetic anisotropy and a system including two ferromagnetic layers with the same thicknesses \$t\$ and saturation magnetizations \$M_s\$, but different magnetic anisotropies \$H_{k,\text{BL}}^{\text{eff}} \neq H_{k,\text{TL}}^{\text{eff}}\$. The effective magnetic field \$\mathbf{H}_i\$ acting on the unit vector of the magnetic moment \$\mathbf{m}_i\$ is given by

$$\mathbf{H}_i = (H_{\text{ext}} + H_{k,i}^{\text{eff}} m_{z,i}) \mathbf{e}_z - H_E \mathbf{m}_j \quad (i \neq j), \quad (\text{B1})$$

where \$H_E = -J_{\text{ex}}/(\mu_0 M_s t)\$ is the exchange field with interlayer exchange coupling energy per unit area \$J_{\text{ex}}\$. The equations of motion for magnetization precessions in each layer can be obtained from the coupled LLG equations:

$$\frac{d\mathbf{m}_i}{dt} = -\mu_0 \gamma \mathbf{m}_i \times (\mathbf{H}_i + \mathbf{h}_{\text{rf}}) + \alpha_i \mathbf{m}_i \times \frac{d\mathbf{m}_i}{dt}, \quad (\text{B2})$$

where \$\alpha_i\$ is the Gilbert damping constant and \$\mathbf{h}_{\text{rf}}\$ is the microwave field. Now, we consider a small oscillation of magnetization around the \$z\$ axis. Using the approximation \$|\delta m_{x,i}|, |\delta m_{y,i}| \ll 1\$, \$\mathbf{m}_i\$ can be expressed as

$$\mathbf{m}_i = (\delta m_{x,i} \mathbf{e}_x + \delta m_{y,i} \mathbf{e}_y) e^{i 2\pi f t} + m_{z,i} \mathbf{e}_z. \quad (\text{B3})$$

Here, we introduce the circular variables \$\delta m_{\pm,i} = \delta m_{x,i} \pm i \delta m_{y,i}\$ and \$h_{\pm} = h_{\text{rf},x} \pm i h_{\text{rf},y}\$, and the linearized LLG equations can be obtained by substituting Eqs. (B1) and (B3) into Eq. (B2).

For the T-T antiparallel magnetization configuration \$m_{z,\text{BL}} = -1, m_{z,\text{TL}} = 1\$, Eq. (B2) becomes

$$\begin{aligned} & \left(\pm \frac{2\pi f}{\mu_0 \gamma} - \tilde{H}_{\text{BL}}^{\text{T-T}} + i\alpha_{\text{BL}} \frac{2\pi f}{\mu_0 \gamma} \right) \delta m_{\pm,\text{BL}} + H_E \delta m_{\pm,\text{TL}} \\ &= h_{\text{rf},\pm}, \end{aligned} \quad (\text{B4})$$

$$\begin{aligned} & -H_E \delta m_{\pm,\text{BL}} + \left(\pm \frac{2\pi f}{\mu_0 \gamma} - \tilde{H}_{\text{TL}}^{\text{T-T}} - i\alpha_{\text{TL}} \frac{2\pi f}{\mu_0 \gamma} \right) \delta m_{\pm,\text{TL}} \\ &= -h_{\text{rf},\pm}, \end{aligned} \quad (\text{B5})$$

where \$\tilde{H}_{\text{BL}}^{\text{T-T}} = H_{\text{ext}} - H_{k,\text{BL}}^{\text{eff}} - H_E\$ and \$\tilde{H}_{\text{TL}}^{\text{T-T}} = H_{\text{ext}} + H_{k,\text{TL}}^{\text{eff}} + H_E\$. For the H-H antiparallel magnetization configuration \$m_{z,\text{BL}} = 1, m_{z,\text{TL}} = -1\$, Eq. (B2) becomes

$$\begin{aligned} & \left(\pm \frac{2\pi f}{\mu_0 \gamma} - \tilde{H}_{\text{BL}}^{\text{H-H}} - i\alpha_{\text{BL}} \frac{2\pi f}{\mu_0 \gamma} \right) \delta m_{\pm,\text{BL}} - H_E \delta m_{\pm,\text{TL}} \\ &= -h_{\text{rf},\pm}, \end{aligned} \quad (\text{B6})$$

$$\begin{aligned} & H_E \delta m_{\pm,\text{BL}} + \left(\pm \frac{2\pi f}{\mu_0 \gamma} - \tilde{H}_{\text{TL}}^{\text{H-H}} + i\alpha_{\text{TL}} \frac{2\pi f}{\mu_0 \gamma} \right) \delta m_{\pm,\text{TL}} \\ &= h_{\text{rf},\pm}, \end{aligned} \quad (\text{B7})$$

where \$\tilde{H}_{\text{BL}}^{\text{H-H}} = H_{\text{ext}} + H_{k,\text{BL}}^{\text{eff}} + H_E\$ and \$\tilde{H}_{\text{TL}}^{\text{H-H}} = H_{\text{ext}} - H_{k,\text{TL}}^{\text{eff}} - H_E\$. The resonance frequencies given in Eqs. (1) and (2) can be obtained by setting the determinant of the system [4 \$\times\$ 4 matrix on the left-hand side of Eqs. (B4)–(B7)] equal to zero, with \$\alpha_{\text{BL}} = \alpha_{\text{TL}} = 0\$.

APPENDIX C: NUMERICAL SIMULATION

The numerical simulations are performed by solving Eq. (B2) using the conventional fourth-order Runge-Kutta algorithm. To excite the magnetic resonance, we apply the microwave field at fixed frequency \$f\$ defined as \$\mathbf{h}_{\text{rf}}(\theta, \delta) \equiv

$h_0(\cos \theta \cos(2\pi ft)\mathbf{e}_x + \sin \theta \cos(2\pi ft + \delta)\mathbf{e}_y)$, where $\mu_0 h_0 = 0.1$ mT. The polarization of the microwave field can then be tuned as $\mathbf{h}_{RH} = \mathbf{h}_{rf}(\pi/4, -\pi/2)$, $\mathbf{h}_{LH} = \mathbf{h}_{rf}(\pi/4, \pi/2)$, $\mathbf{h}_x = \mathbf{h}_{rf}(0, 0)$, or $\mathbf{h}_y = \mathbf{h}_{rf}(\pi/2, 0)$. In the calculation shown in Fig. 5(b), we initially assign the magnetization state in the H-H antiparallel magnetization configuration $m_{z,BL} = 1, m_{z,TL} = -1$, and then calculate the precession amplitude of the total magnetization \mathbf{m} at each point of the applied magnetic field.

-
- [1] V. V. Kruglyak, S. O. Demokritov, and D. Grundler, Magnonics, *J. Phys. D: Appl. Phys.* **43**, 264001 (2010).
- [2] A. V. Chumak, V. I. Vasyuchka, A. A. Serga, and B. Hillebrands, Magnon spintronics, *Nat. Phys.* **11**, 453 (2015).
- [3] H. Yu, J. Xiao, and H. Schultheiss, Magnetic texture based magnonics, *Phys. Rep.* **905**, 1 (2021).
- [4] T. Schneider, A. A. Serga, B. Leven, B. Hillebrands, R. L. Stamps, and M. P. Kostylev, Realization of spin-wave logic gates, *Appl. Phys. Lett.* **92**, 022505 (2008).
- [5] A. Khitun, M. Bao, and K. L. Wang, Magnonic logic circuits, *J. Phys. D: Appl. Phys.* **43**, 264005 (2010).
- [6] A. Khitun and K. L. Wang, Non-volatile magnonic logic circuits engineering, *J. Appl. Phys.* **110**, 034306 (2011).
- [7] N. Sato, K. Sekiguchi, and Y. Nozaki, Electrical demonstration of spin-wave logic operation, *Appl. Phys. Express* **6**, 063001 (2013).
- [8] M. Jamali, J. H. Kwon, S.-M. Seo, K.-J. Lee, and H. Yang, Spin wave nonreciprocity for logic device applications, *Sci. Rep.* **3**, 3160 (2013).
- [9] R. Nakane, G. Tanaka, and A. Hirose, Reservoir computing with spin waves excited in a garnet film, *IEEE Access* **6**, 4462 (2018).
- [10] T. Brächer and P. Pirro, An analog magnon adder for all-magnonic neurons, *J. Appl. Phys.* **124**, 152119 (2018).
- [11] Á Papp, W. Porod, and G. Csaba, Nanoscale neural network using non-linear spin-wave interference, *Nat. Commun.* **12**, 6422 (2021).
- [12] Q. Wang, A. V. Chumak, and P. Pirro, Inverse-design magnonic devices, *Nat. Commun.* **12**, 2636 (2021).
- [13] A. Mahmoud, F. Ciubotaru, F. Vanderveken, A. V. Chumak, S. Hamdioui, C. Adelmann, and S. Cotofana, Introduction to spin wave computing, *J. Appl. Phys.* **128**, 161101 (2020).
- [14] F. Keffer and C. Kittel, Theory of antiferromagnetic resonance, *Phys. Rev.* **85**, 329 (1952).
- [15] A. G. Gurevich and G. A. Melkov, *Magnetization Oscillations and Waves* (CRC Press, Boca Raton, FL, 1996).
- [16] R. Cheng, M. W. Daniels, J. Zhu, and D. Xiao, Antiferromagnetic spin wave field-effect transistor, *Sci. Rep.* **6**, 24223 (2016).
- [17] J. Lan, W. Yu, and J. Xiao, Antiferromagnetic domain wall as spin wave polarizer and retarder, *Nat. Commun.* **8**, 178 (2017).
- [18] M. W. Daniels, R. Cheng, W. Yu, J. Xiao, and D. Xiao, Nonabelian magnonics in antiferromagnets, *Phys. Rev. B* **98**, 134450 (2018).
- [19] W. Yu, J. Lan, and J. Xiao, Polarization-selective spin wave driven domain-wall motion in antiferromagnets, *Phys. Rev. B* **98**, 144422 (2018).
- [20] W. Yu, J. Lan, and J. Xiao, Magnetic logic gate based on polarized spin waves, *Phys. Rev. Appl.* **13**, 024055 (2020).
- [21] J. Li, *et al.*, Spin current from sub-terahertz-generated antiferromagnetic magnons, *Nature* **578**, 70 (2020).
- [22] P. Vaidya, S. A. Morley, J. Van Tol, Y. Liu, R. Cheng, A. Brataas, D. Lederman, and E. Del Barco, Subterahertz spin pumping from an insulating antiferromagnet, *Science* **368**, 160 (2020).
- [23] P. Grünberg, R. Schreiber, Y. Pang, M. B. Brodsky, and H. Sowers, Layered Magnetic Structures: Evidence for Anti-ferromagnetic Coupling of Fe Layers across Cr Interlayers, *Phys. Rev. Lett.* **57**, 2442 (1986).
- [24] M. N. Baibich, J. M. Broto, A. Fert, F. N. Van Dau, F. Petroff, P. Etienne, G. Creuzet, A. Friederich, and J. Chazelas, Giant Magnetoresistance of (001)Fe/(001)Cr Magnetic Superlattices, *Phys. Rev. Lett.* **61**, 2472 (1988).
- [25] S. S. P. Parkin, Systematic Variation of the Strength and Oscillation Period of Indirect Magnetic Exchange Coupling through the 3d, 4d, and 5d Transition Metals, *Phys. Rev. Lett.* **67**, 3598 (1991).
- [26] R. A. Duine, K. Lee, S. S. P. Parkin, and M. D. Stiles, Synthetic antiferromagnetic spintronics, *Nat. Phys.* **14**, 217 (2018).
- [27] S. Yakata, H. Kubota, T. Sugano, T. Seki, K. Yakushiji, A. Fukushima, S. Yuasa, and K. Ando, Thermal stability and spin-transfer switchings in MgO-based magnetic tunnel junctions with ferromagnetically and antiferromagnetically coupled synthetic free layers, *Appl. Phys. Lett.* **95**, 242504 (2009).
- [28] X. M. Liu, H. T. Nguyen, J. Ding, M. G. Cottam, and A. O. Adeyeye, Interlayer coupling in Ni₈₀Fe₂₀/Ru/Ni₈₀Fe₂₀ multilayer films: Ferromagnetic resonance experiments and theory, *Phys. Rev. B* **90**, 064428 (2014).
- [29] S. H. Yang, K. S. Ryu, and S. Parkin, Domain-wall velocities of up to 750 m s⁻¹ driven by exchange-coupling torque in synthetic antiferromagnets, *Nat. Nanotechnol.* **10**, 221 (2015).
- [30] T. Dohi, S. DuttaGupta, S. Fukami, and H. Ohno, Formation and current-induced motion of synthetic antiferromagnetic skyrmion bubbles, *Nat. Commun.* **10**, 5153 (2019).
- [31] R. A. Gallardo, *et al.*, Reconfigurable Spin-Wave Nonreciprocity Induced by Dipolar Interaction in a Coupled Ferromagnetic Bilayer, *Phys. Rev. Appl.* **10**, 034012 (2019).
- [32] M. Ishibashi, Y. Shiota, T. Li, S. Funada, T. Moriyama, and T. Ono, Switchable giant nonreciprocal frequency shift of propagating spin waves in synthetic antiferromagnets, *Sci. Adv.* **6**, eaaz6931 (2020).
- [33] Y. Shiota, T. Taniguchi, M. Ishibashi, T. Moriyama, and T. Ono, Tunable magnon-magnon coupling mediated by dynamic dipolar interaction in synthetic antiferromagnets, *Phys. Rev. Lett.* **125**, 017203 (2020).
- [34] A. Sud, C. W. Zollitsch, A. Kamimaki, T. Dion, S. Khan, S. Iihama, S. Mizukami, and H. Kurebayashi, Tunable magnon-magnon coupling in synthetic antiferromagnets, *Phys. Rev. B* **102**, 100403(R) (2020).

- [35] M. Ishibashi, Y. Shiota, S. Funada, T. Moriyama, and T. Ono, Spin wave resonance in perpendicular magnetized synthetic antiferromagnets, *J. Magn. Soc. Jpn.* **45**, 25 (2021).
- [36] J. Diaz, S. Haraldson, U. Smith, and L. Pettersson, A microwave cavity for circularly polarized radiation, *Rev. Sci. Instrum.* **45**, 454 (1974).
- [37] J. J. Henderson, C. M. Ramsey, H. M. Quddusi, and E. Del Barco, High-frequency microstrip cross resonators for circular polarization electron paramagnetic resonance spectroscopy, *Rev. Sci. Instrum.* **79**, 074704 (2008).
- [38] M. Curcic, *et al.*, Polarization Selective Magnetic Vortex Dynamics and Core Reversal in Rotating Magnetic Fields, *Phys. Rev. Lett.* **101**, 197204 (2008).
- [39] H. Suto, T. Kanao, T. Nagasawa, K. Kudo, K. Mizushima, and R. Sato, Subnanosecond microwave-assisted magnetization switching in a circularly polarized microwave magnetic field, *Appl. Phys. Lett.* **110**, 262403 (2017).
- [40] A. Bisig, *et al.*, Dynamic domain wall chirality rectification by rotating magnetic fields, *Appl. Phys. Lett.* **106**, 122401 (2015).
- [41] I. Kan, Y. Soeno, T. Roppongi, and Y. Nozaki, Circularly polarized magnetic field generated by two microfabricated crossed coplanar waveguides, *Appl. Phys. Lett.* **110**, 202404 (2017).
- [42] H. Suto, T. Kanao, T. Nagasawa, K. Mizushima, R. Sato, N. Kikuchi, and S. Okamoto, Microwave-magnetic-field-induced magnetization excitation and assisted switching of antiferromagnetically coupled magnetic bilayer with perpendicular magnetization, *J. Appl. Phys.* **125**, 153901 (2019).
- [43] G. H. O. Daalderop, P. J. Kelly, and F. J. A. Den Broeder, Prediction and Confirmation of Perpendicular Magnetic Anisotropy in Co/Ni Multilayers, *Phys. Rev. Lett.* **68**, 682 (1992).
- [44] J. M. Beaujour, D. Ravelosona, I. Tudosa, E. E. Fullerton, and A. D. Kent, Ferromagnetic resonance linewidth in ultrathin films with perpendicular magnetic anisotropy, *Phys. Rev. B* **80**, 180415(R) (2009).
- [45] J. Han, P. Zhang, J. T. Hou, S. A. Siddiqui, and L. Liu, Mutual control of coherent spin waves and magnetic domain walls in a magnonic device, *Science* **366**, 1121 (2020).
- [46] T. Arakawa, Y. Shiota, K. Yamada, T. Ono, and S. Kon, Magnetic polarization selective spectroscopy of magnetic thin films probed by wideband crossed microstrip circuit in GHz regime, *Rev. Sci. Instrum.* **93**, 013901 (2022).
- [47] T. Devolder, Ferromagnetic resonance of exchange-coupled perpendicularly magnetized bilayers, *J. Appl. Phys.* **119**, 153905 (2016).
- [48] X. Chen, C. Zheng, Y. Zhang, S. Zhou, Y. Liu, and Z. Zhang, Identification and manipulation of spin wave polarizations in perpendicularly magnetized synthetic antiferromagnets, *New J. Phys.* **23**, 113029 (2021).